Title

THE K+p INTERACTION FROM 864 TO 1585 MeV/c; CROSS SECTIONS AND MASS DISTRIBUTIONS

Authors

Bland, Roger W.
Bowler, Michael G.
Brown, John L.
et al.

Publication Date

1969-05-01

Submitted to Nuclear Physics B

UCRL-18758
Preprint

eyl.2

THE K^+p INTERACTION FROM 864 to 1585 MeV/c; CROSS SECTIONS AND MASS DISTRIBUTIONS

Roger W. Bland, Michael G. Bowler, John L. Brown
John A. Kadyk, Gerson Goldhaber, Sulamith Goldhaber
Victor H. Seeger, and George H. Trilling

May 1969

AEC Contract No. W-7405-eng-48

LAWRENCE RADIATION LABORATORY
UNIVERSITY of CALIFORNIA BERKELEY

eyl.1

UCRL-18758

DISCLAIMER

THE K^+p INTERACTION FROM 864 to 1585 MeV/c; CROSS SECTIONS AND MASS DISTRIBUTIONS†

Roger W. Bland, Michael G. Bowler††, John L. Brown†††, John A. Kadyk, Gerson Goldhaber, Sulamith Goldhaber‡, Victor H. Seeger, and George H. Trilling

Department of Physics and Lawrence Radiation Laboratory
University of California, Berkeley, California 94720

May 1969

ABSTRACT

In this paper we present, for five momenta from 864 to 1585 MeV/c, cross sections for stable final states and for resonance production, and an analysis of the $KN\pi$ Dalitz plots including the effects of $K^*(891)$-$\Delta(1236)$ interference. We see strong interference at all momenta where the K^* is present, with the relative phase of the K^*N and $K\Delta$ amplitudes remaining constant as a function of momentum. We combine our cross-section results with those from other experiments to study the momentum dependence of the partial cross sections in the region of the 1250-MeV/c peak in the total cross section; we find that the total cross-section curve can be represented as the sum of partial cross-section curves, each one smooth and without a peak corresponding to that in the total cross section. Thus this structure is not due to structure

---

†Work done under the auspices of the U.S. Atomic Energy Commission.

††Present address: Nuclear Physics Laboratory, Oxford, England.

†††Present address: Stanford Linear Acceleration Center, Stanford, California.

‡Deceased.

in any single partial cross section, but rather to the sharp rises of the single- and double-pion-production channels at widely separated thresholds. This interpretation is at variance with a conventional resonance interpretation of the observed structure in the total cross section.

1. INTRODUCTION

In meson-baryon scattering the KN system is unique in having no well-established direct-channel resonances. The KN cross sections are the smallest of the meson-baryon cross sections, and show the least structure as a function of energy. This is perhaps related to the fact that a KN resonant state could not belong to the well-known singlet, octet, or decuplet representations of SU(3), but would require an exotic representation such as $\overline{10}$ or 27, for which there is no other compelling experimental evidence. In terms of the quark model at least five quarks would be required, $qqqq\bar{q}$, instead of the usual three-quark representation of baryon states.

This experiment was orginally planned as a detailed investigation of K^+p interactions from 860 to 1585 MeV/c, just above the inelastic threshold. The K^+p cross section was known to rise sharply from 11 mb to 18 mb in this momentum interval, leveling off at higher momenta.[1, 21, 24] Recent precise measurements by Cool et al.[2, 3] and Bugg et al.[4] show a small($\approx$ 1 mb) peak at about 1250 MeV/c beam momentum†. If interpreted as a resonance it would be strangeness +1 baryon (Z^*) with mass 1910 MeV, width 180 MeV, and isotopic spin 1, belonging to a 27-dimensional representation of SU(3).

In this paper, one of a series of detailed papers on K^+p interactions between 864 and 1585 MeV/c, we discuss cross sections, including those for resonance production, at 864, 969, 1207, 1367, and 1585 MeV/c. Another paper of the series is on elastic scattering at 864, 969 and 1207 MeV/c,[5] and a subsequent paper will discuss the detailed properties of inelastic final

†The values of σ_t that we used differ slightly from those given in Ref. [2] and were supplied by T. Kycia on November 15, 1967.

states. Several preliminary results have been published in earlier papers.[6-9])

2. DESCRIPTION OF THE EXPERIMENT

The film for this experiment was taken in the Lawrence Radiation Laboratory 25-inch bubble chamber filled with hydrogen. Positive kaons were supplied by a two-stage variable-momentum mass-separated beam.[10]) The target was in an extracted proton beam, external to the Bevatron field, permitting operation over a wide range of momenta with positive or negative particles. Below 1207 MeV/c, the K^+ beam was pure to less than 1%, but at the higher momenta there was some contamination of the kaon beam, rising from 2% at 1207 MeV/c to 15% at 1585 MeV/c. The momentum bite was about ± 3/4%.

In Table 1 we give the number of pictures and the number of events of each topology analyzed at each momentum. The momenta given in this table are average fitted beam momenta at the point of the K^+ interaction or decay. The primary measuring device for this experiment was the Berkeley Flying Spot Digitizer (FSD),[11]) a rapid automatic machine measuring at a rate of about 100 events an hour. Two "Franckenstein" hand-operated measuring projectors were also used, mainly for remeasurements. The measurements were analyzed with two sequences of programs, both using two-view reconstruction; the FOG-CLOUDY-FAIR system, for FSD measurements, and PACKAGE, for the Franckenstein measurements. The only unconventional feature of the fitting was "total beam-track editing" of FSD events. In this procedure the measured beam momentum and angles were replaced by average values derived from a subsample of events with well-measured beam tracks,

Table 1. Number of pictures taken and numbers of events analyzed.

Beam momentum (MeV/c)	Number of pictures	Number of events				
		3-prong	2-prong, no V^0	2-prong, with V^0	4-prong	Total
864	46 000	2 300	13 000	350	20	15 670
969	25 000	1 100	8 100	500	30	9 730
	17 000[a]	--	--	200	--	200
1 207	44 000	1 100	12 600	1 100	50	14 850
1 367	66 000	1 500	--	1 800	400	3 700
1 585	51 000	700	--	1 000	900	2 600
all	249 000	6 700	33 700	4 950	1 400	46 750

[a]Only V^0 events were measured in this section of film.

using as errors the half-widths of the fitted beam momentum and angular distributions for the subsample. This procedure was followed because the large incident particle flux, 15 to 25 kaons per frame, caused a high failure rate for FSD beam-track measurements. Total beam editing was not necessary for Franckenstein measurements, since the correct beam track could usually be satisfactorily located by the operator.

After measuring, fitting, and inspection of ionization where necessary, all events were either accepted, remeasured, or rejected as one of a number of distinct reject types. Since the production of two missing neutrals is very small in our momentum range, nearly all well-measured events were expected to fit some kinematically constrained hypothesis. For an event to be accepted it was first required that all secondary tracks be well measured, as indicated by the spread of measured points from the fitted curve. A kinematic-fitting χ^2 cutoff was then made, at $\chi^2 = 20$ for elastic scatterings (confidence level = 0.06%) and at the 1% confidence level for other hypotheses. Events fitting only one four-constraint hypothesis (no missing neutrals) were accepted regardless of whether any of the one-constraint hypotheses (one missing neutral) gave a fit. A check of this procedure on about one-third of such events, by inspection of ionization, revealed no instance in which a one-constraint fit should have been chosen. Ambiguities among four-constraint hypotheses were always resolved by inspection of ionization. Events with no four-constraint fit were looked at on the scan table, and ambiguities among one-constraint hypotheses remaining after inspection of ionization were always less than 2% of the inelastic events. In the case of ambiguities between incident-K^+ and incident-π^+ hypotheses at the same constraint level the incident-K^+ was always chosen.

After several rounds of remeasuring, the original sample of events was resolved as follows:

Accepted	84%
Ambiguous	0.05%
Unresolved (because of repeated measurement failures)	2.5%
Unbiased FSD failures (not remeasured)	7%
Nonbeam	4%
Fake events	1.6%
No-fits	0.4%
Zero-constraint	0.2%

For the purpose of computing cross sections the unresolved events and unbiased FSD failures were distributed within each topology proportionally to the numbers of accepted events in the various reactions. We discarded the nonbeam events, "fake" events (mainly duplicates), and no-fit events (mainly events arising from off-momentum incident particles). The zero-constraint events, due to secondary scattering or decays near the primary vertex, were redistributed among the appropriate one-constraint hypotheses. For further details of the analysis procedures see Refs. [12]) and [13]).

3. DETERMINATION OF CROSS SECTIONS

In this section we discuss cross sections for final states stable with respect to the strong interactions; resonance-production cross sections are discussed in the following section. Our results are summarized in Tables 2a-e. A subsample of the film was chosen at each momentum for cross-section

Table 2a. Corrected numbers of events and cross sections, 864 MeV/c.

Reaction	Corrected number of events	Cross Section: Decay normalization (mb)	Cross Section: Counter normalization (mb)
$K^+p \rightarrow K^+p$, $\cos\theta_{cm} < 0.9$	11234 ± 173		
$\rightarrow K^+p$, all $\cos\theta_{cm}$, nuclear only	11608 ± 190	12.37 ± 0.49	11.98 ± 0.27
$K^+p \rightarrow K^0p\pi^+$	1112 ± 48	1.19 ± 0.07	1.15 ± 0.06
$\rightarrow K^+p\pi^0$	351 ± 27	0.37 ± 0.03	0.36 ± 0.03
$\rightarrow K^+n\pi^+$	127 ± 16	0.135 ± 0.018	0.131 ± 0.017
$\rightarrow KN\pi$	1590 ± 57	1.70 ± 0.09	1.64 ± 0.07
$K^+p \rightarrow$ all final states	13198 ± 198	14.07 ± 0.55	13.62 ± 0.30
$K^+ \rightarrow \pi^+\pi^+\pi^-$	2220 ± 68		

Table 2b. Corrected numbers of events and cross sections, 969 MeV/c.

Reaction	Corrected number of events	Cross Section: Decay normalization (mb)	Cross Section: Counter normalization (mb)
$K^+p \rightarrow K^+p$, $\cos\theta_{cm} < 0.9$	3848 ± 95		
$\rightarrow K^+p$, all $\cos\theta_{cm}$, nuclear only	4063 ± 107	11.63 ± 0.71	11.68 ± 0.21
$K^+p \rightarrow K^0p\pi^+$	895 ± 43	2.56 ± 0.19	2.57 ± 0.12
$\rightarrow K^+p\pi^0$	277 ± 24	0.79 ± 0.08	0.80 ± 0.07
$\rightarrow K^+n\pi^+$	104 ± 14	0.30 ± 0.04	0.30 ± 0.04
$\rightarrow KN\pi$	1276 ± 51	3.65 ± 0.25	3.67 ± 0.14
$K^+p \rightarrow$ all final states	5339 ± 118	15.28 ± 0.90	15.35 ± 0.22
$K^+ \rightarrow \pi^+\pi^+\pi^-$	737 ± 38		

Table 2c. Corrected numbers of events and cross sections, 1207 MeV/c.

Reaction	Corrected number of events	Cross section	
		Decay normalization (mb)	Counter normalization (mb)
$K^+p \to K^+p$, $\cos\theta_{cm} < 0.9$	3671 ± 101		
$\to K^+p$, extrapolated	4252 ± 105	11.81 ± 0.79	10.89 ± 0.18
$K^+p \to K^0p\pi^+$	1966 ± 66	5.46 ± 0.38	5.04 ± 0.15
$\to K^+p\pi^0$	704 ± 39	1.95 ± 0.16	1.80 ± 0.10
$\to K^+n\pi^+$	219 ± 22	0.61 ± 0.07	0.56 ± 0.06
$\to KN\pi$	2889 ± 80	8.02 ± 0.54	7.40 ± 0.17
$K^+p \to K^+p\pi^+\pi^-$	10 ± 4	0.028 ± 0.011	0.026 ± 0.010
$K^+p \to$ all final states	7151 ± 132	19.85 ± 1.28	18.32 ± 0.12
$K^+ \to \pi^+\pi^+\pi^-$	610 ± 36		

Table 2d. Corrected numbers of events and cross sections, 1367 MeV/c.

Reaction	Corrected number of events	Cross section, decay normalization (mb)
$K^+p \to K^0p\pi^+$, $K^0 \to \pi^+\pi^-$	1796 ± 72	
$\to K^0p\pi^+$, all K^0 decays	5256 ± 224[a]	5.36 ± 0.33
$\to K^+p\pi^+\pi^-$	64 ± 11	0.065 ± 0.012
$K^+p \to K^0p\pi^+\pi^0$, $K^0 \to \pi^+\pi^-$	20 ± 6	
$\to K^0p\pi^+\pi^0$, all K^0 decays	58.6 ± 17.6[a]	0.060 ± 0.018
$\to K^0n\pi^+\pi^+$, $K^0 \to \pi^+\pi^-$	$3\ ^{+4}_{-2}$	
$\to K^0n\pi^+\pi^+$, all K^0 decays	$8.8\ ^{+12}_{-6}$[a]	$0.009\ ^{+0.012}_{-0.006}$
$K^+ \to \pi^+\pi^+\pi^-$	1467 ± 59	

[a] We take $R(K^0 \to \pi^+\pi^-)/R(K^0 \to \text{all modes}) = 0.342 \pm 0.005$, from Ref. [16].

Table 2e. Corrected numbers of events and cross sections, 1585 MeV/c.

Reaction	Corrected number of events	Cross section, decay normalization (mb)
$K^+p \to K^0p\pi^+$, $K^0 \to \pi^+\pi^-$	789 ± 40	
$\to K^0p\pi^+$, all K^0 decays	2307 ± 122[a]	5.0 ± 0.4
$K^+p \to K^+p\pi^+\pi^-$	172 ± 19	0.38 ± 0.05
$\to K^0p\pi^+\pi^0$, $K^0 \to \pi^+\pi^-$	50 ± 10	
$\to K^0p\pi^+\pi^0$, all K^0 decays	146 ± 29[a]	0.32 ± 0.07
$\to K^0n\pi^+\pi^+$, $K^0 \to \pi^+\pi^-$	13 ± 5	
$\to K^0n\pi^+\pi^+$, all K^0 decays	38 ± 15[a]	0.08 ± 0.03
$K^+p \to K^+p\pi^+\pi^-\pi^0$	$4^{+4.5}_{-2.5}$	$0.009^{+0.010}_{-0.005}$
$\to K^0p\pi^+\pi^-\pi^+$	3^{+7}_{-2}	$0.006^{+0.015}_{-0.004}$
$K^+ \to \pi^+\pi^+\pi^-$	590 ± 34 events	

a. We take $R(K^0 \to \pi^+\pi^-)/R(K^0 \to \text{all modes}) = 0.342 \pm 0.005$, from Ref. [16].

determination; at 864, 1367, and 1585 MeV/c most of the film was used, and at 969 and 1207 MeV/c, slightly less than half. The numbers in Tables 2a-e refer to these selected cross-section samples, and the numbers of events in Table 1 refer to the entire sample of film analyzed. In the analysis of resonance production the entire sample was used.

Before presenting cross sections we consider small corrections for several experimental biases: beam contamination, scanning loss, K_1^0 escape loss, and Coulomb effects and loss of short protons in elastic scattering.

A. Beam Contamination

There is little contamination at momenta below 1207 MeV/c, but at the higher momenta pion contamination becomes a significant problem. Because of this problem, at 1367 and 1585 MeV/c only 3-prong events (K^+ decays), 4-prong events, and events with a visible V^0 decay were measured. The 3-prong and V^0 topologies are not easily simulated by incident pions, and were assumed to be free of contamination. The 4-prong events were substantially contaminated by incident pions but the separation of K^+ events from π^+ events by fitting and inspection of ionization was quite adequate for the small number of events observed. The 2-prongs were measured only at or below 1207 MeV/c, and at 1207 MeV/c a correction for pion contamination was made. For this purpose events from half of a roll of 1207-MeV/c incident-π film, exposed at the time of the K^+p run, were measured. These events were processed in the same way as 2-prongs in the K^+ film. About 30% fitted as apparent K^+-induced events, and the remainder fitted only as π^+-induced events. From the number of events in the K^+ film identified uniquely as π^+-induced events, it was then possible to deduce the number of π^+ events

incorrectly identified as K^+ events. These were substracted from the final states of the 2-prong topology, in proportion to the numbers of accepted K^+ events in the incident-π^+ sample. At 864 and 969 MeV/c the pion contamination was negligible even in the 2-prong topology.

B. Scanning Biases

At each momentum a sample of film was rescanned, and a topology-dependent correction was made for each reaction. The single-scan efficiency ranged from 90% to 97%, varying with topology and momentum.

C. Short-Proton Loss and Coulomb Correction

Elastic scattering events with short recoil proton tracks become increasingly difficult to detect as the scattering angle decreases. For K^+p elastic scattering with $\cos\theta_{c.m.} = 0.9$, the recoiling proton has a stopping range of 11.6, 17.0, or 29 cm, at 864, 969, or 1207 MeV/c, respectively. To minimize the short-proton bias we deleted from our sample elastic scattering events with $\cos\theta > 0.9$, and measured the cross section for elastic scattering with $-1 < \cos\theta < 0.9$. We then calculated a cross section for nuclear elastic scattering at all angles. This required a correction for Coulomb effects and an extrapolation of the cross section to $0.9 < \cos\theta < 1.0$, both of which are model-dependent. At 864 and 969 MeV/c we used for this purpose the partial-wave amplitudes from our phase-shift analysis of the elastic scattering events.[14] The nuclear cross section so obtained is lower by 0.4 mb at 864 MeV/c and by 0.2 mb at 969 MeV/c than that obtained by extrapolating the uncorrected data from $\cos\theta = 0.9$ to $\cos\theta = 1$. At 1207 MeV/c we merely extrap-

olated with a third-order Legendre fit.

D. Escape Correction

The typical K_1^0 decay length in our experiment was small compared with the chamber dimensions, and K_1^0 escape corrections amounted to only 1% and 2.6% at 1367 and 1585 MeV/c respectively. No correction was necessary at lower momenta, since the lost V^0 events were analyzed in the 2-prong, no-V^0 topology.

E. Estimation of Errors

We have calculated the statistical error on the number of events in each reaction. Since the statistical uncertainty in the corrections was fairly small, the final statistical error is approximately $N^{1/2}$, where N is the number of events. To take account of possible systematic errors we introduced an arbitrary "systematic error" of $N^{1/2}$, to be added in quadrature to the statistical error. The resulting error was thus taken as approximately equal to $(2N)^{1/2}$.

The corrected numbers of events in the samples of film used for cross-section determination are given in Tables 2a-e.

F. Cross Sections

At each momentum we determined the number of decays of K^+ beam particles via the τ decay mode, $K^+ \rightarrow \pi^+\pi^+\pi^-$, by measuring and fitting 3-prong events. The cross sections normalized to τ decays were calculated from the formula

$$\sigma = \frac{N_{interaction}}{N_{decay}} \times \frac{B}{\eta c \tau} \times \frac{A_H}{\rho_{H_2} N_A} ,$$

where

A_H (atomic weight of hydrogen) = 1.008,

N_A (Avogadro's number) = 6.0248×10^{23} mole^{-1},

ρ_{H_2} (density of hydrogen in the bubble chamber†) =

(0.0608 ± 0.0010) g/cm^3,

$\eta = p_{beam}/M_{K^+}$,

$c = 2.998 \times 10^{10}$ cm/sec,

τ (K^+ lifetime) = 1.235×10^{-8} sec [16]),

B (K^+ branching ratio into the τ decay mode) = 0.0557 ± 0.0004 [16]).

The resulting cross sections are given in Tables 2a-e.

At 864, 969, and 1207 MeV/c we have also computed cross sections normalized to a smoothed version of the total cross section measurements by Cool et al. [2, 3]) and Bugg et al. [4]) (see Fig. 11). For the error on the total cross section we used the smaller of the statistical errors given by the two counter groups. This error is statistical only, and future changes in the cross-section values comparable to the statistical error due to improved analysis of systematic effects cannot be ruled out.

†The density of hydrogen was determined by measuring the stopping length of a muon from the two-body decay of a pion at rest, $\pi^+ \rightarrow \mu^+ + \nu$; Ref. [15]).

4. CROSS SECTIONS FOR RESONANCE PRODUCTION

Inelastic K^+p interactions in the momentum region of our experiment are dominated by a few simple processes:

single pion production,

$$K^+p \rightarrow K^0p\pi^+, \quad (1)$$

$$\rightarrow K^+p\pi^0, \quad (2)$$

$$\rightarrow K^+n\pi^+; \quad (3)$$

and double pion production,

$$K^+p \rightarrow K^+p\pi^+\pi^-, \quad (4)$$

$$\rightarrow K^0p\pi^+\pi^0, \quad (5)$$

$$\rightarrow K^0n\pi^+\pi^+, \quad (6)$$

$$\rightarrow K^+p\pi^0\pi^0 \text{ (underconstrained)}, \quad (7)$$

$$\rightarrow K^+n\pi^+\pi^0 \text{ (underconstrained)}. \quad (8)$$

We discuss only the first six reactions, as the last two reactions have two missing neutrals and are therefore not kinematically constrained. In this section we use the mass distributions for the inelastic final states to determine the various resonance-production cross sections.

A. Single-Pion Production

1. Models Considered

The Dalitz plots for the single-pion-production reactions are shown in Figs. 1-4[†]. In the $K^0\pi^+p$ Dalitz plots at 1207, 1367, and 1585 MeV/c we see a clear dominance of the quasi-two-body final states:

[†]Numerical tabulations of Dalitz plot populations and other data are given in Ref. [17]).

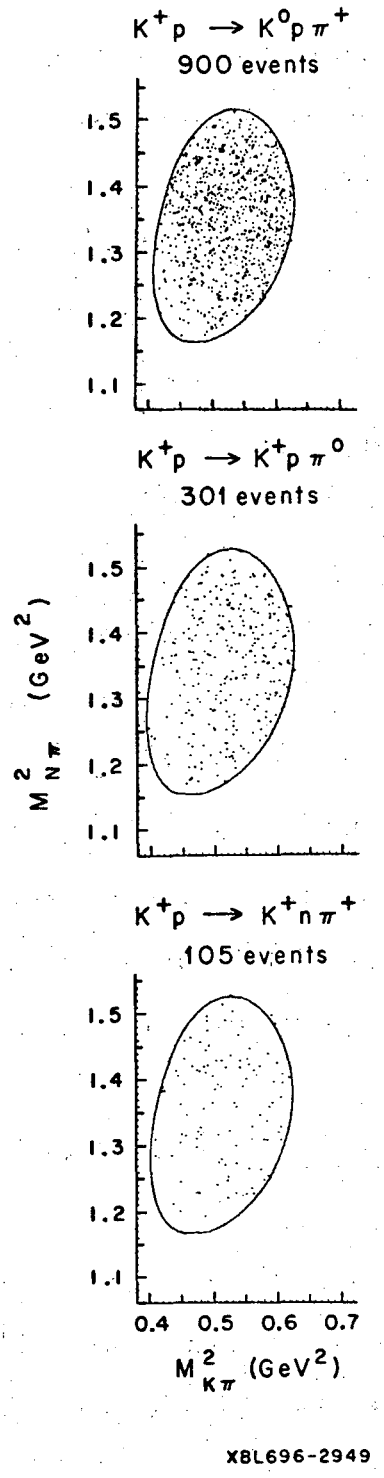

Fig. 1. Single-pion-production Dalitz plots at 864 MeV/c.

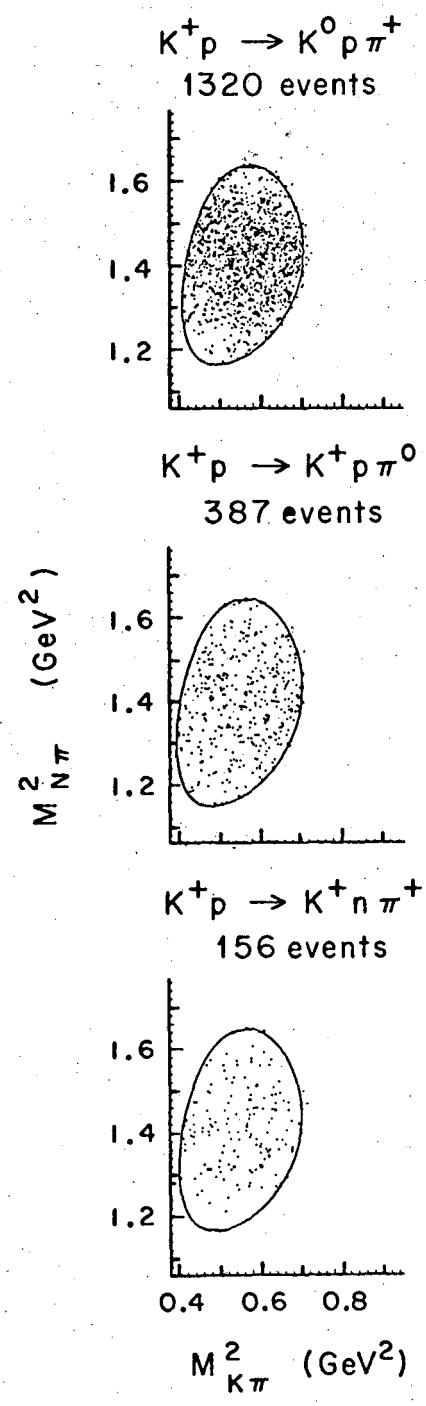

Fig. 2. Single-pion-production Dalitz plots at 969 MeV/c.

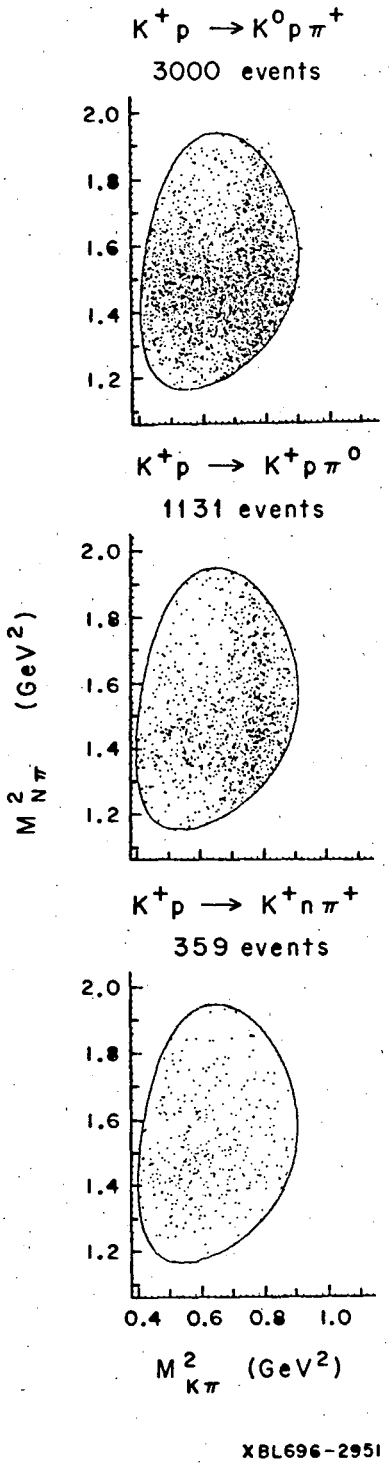

Fig. 3. Single-pion-production Dalitz plots at 1207 MeV/c.

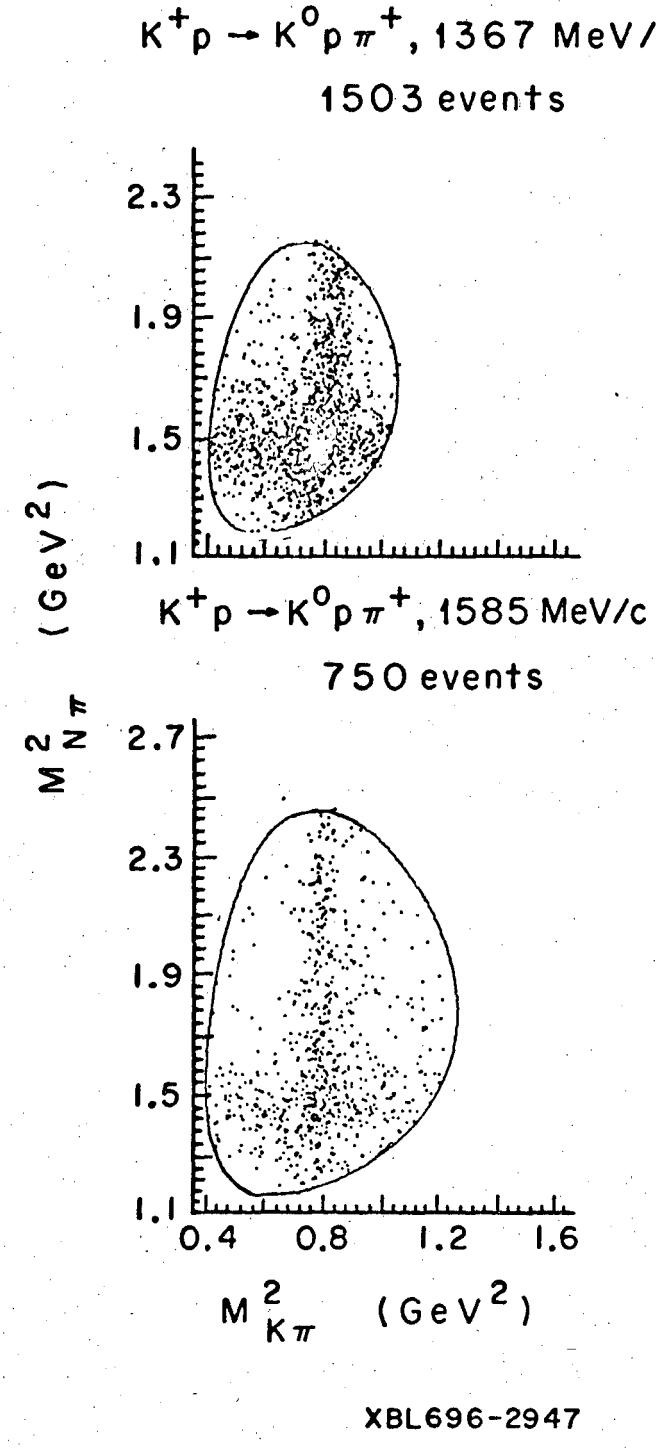

Fig. 4. Single-pion-production Dalitz plots at 1367 and 1585 MeV/c.

$$K^+p \to K\Delta(1236)$$
$$\quad\quad\quad\quad \hookrightarrow \pi N\ ,$$
$$K^+p \to K^*(891)N$$
$$\quad\quad \hookrightarrow K\pi\ .$$

The resonance bands are well defined, and there appears to be little nonresonant background. The 1207-MeV/c data seem to show constructive interference at the crossing of the Δ and K^* bands. At 864 and 969 MeV/c, below K^* threshold and near the Δ threshold, there are no clear resonance bands, since the 120-MeV-wide Δ covers the entire Dalitz plots. It will be shown, however, that Δ production dominates at these momenta as well. In order to draw quantitative conclusions from the Dalitz plots one must construct a model for the single-pion-production reaction. We will consider three models: a noninterference model which we expect to be valid only in the part of the Dalitz plot outside the K^*-Δ overlap region; an empirical model including K^*-Δ interference; and a specific partial-wave model involving assumptions as to the $K\Delta$ and K^*N amplitudes.

a. Noninterference Model

One can represent the Dalitz plot density for production of a single resonance rather generally as the product of a Breit-Wigner function, a production angular momentum barrier factor, and a function specifying the density distribution within the resonance band along a line of fixed resonance mass. The latter function, whose form is determined by the spin of the decaying resonance, is usefully represented in terms of an angle λ. For the $N\pi$ system, we define $\lambda_{N\pi}$ as the decay angle, in the $N\pi$ c.m., of the pion with respect to the outgoing kaon, as shown in Fig. 5. Along a line of constant

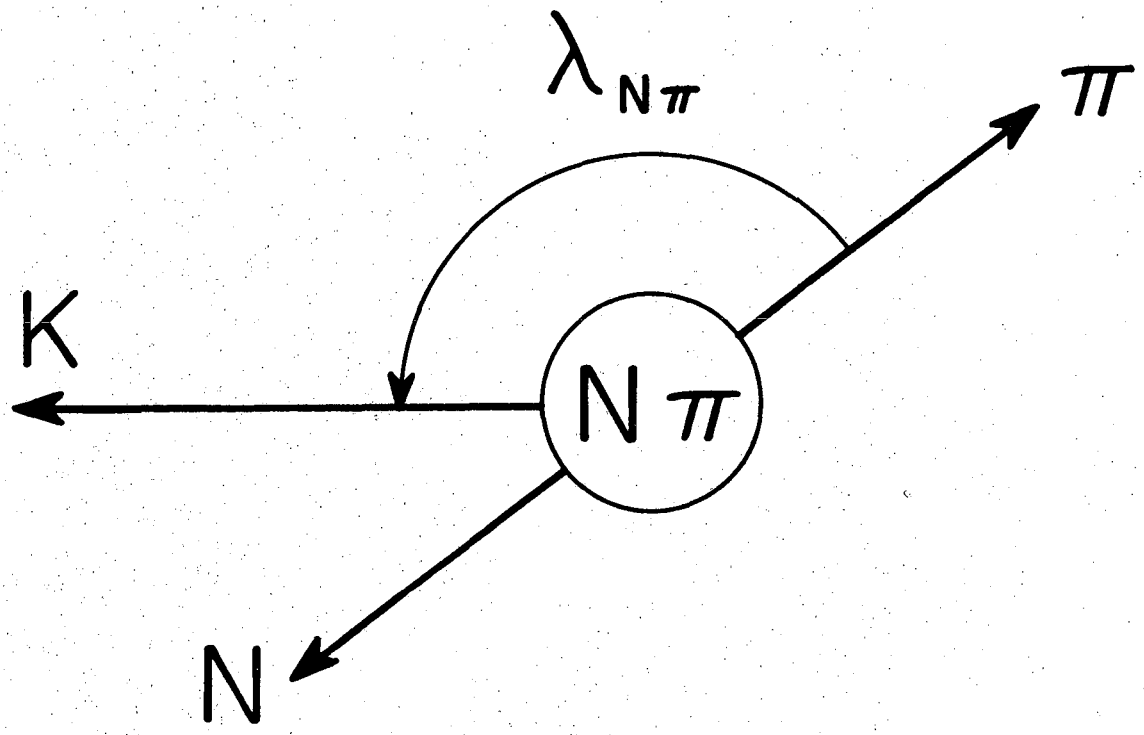

Fig. 5. Definition of $\lambda_{N\pi}$, the pion decay angle in the $N\pi$ c.m. with respect to the direction of the outgoing kaon.

$M^2_{N\pi}$, $M^2_{K\pi}$ varies linearly with $\cos \lambda_{N\pi}$, where $\cos \lambda_{N\pi} = \pm 1$ corresponds to the edges of the Dalitz plot. For the $K\pi$ system we similarly define $\lambda_{K\pi}$ as the decay angle of the pion with respect to the outgoing nucleon, in the $K\pi$ c. m. Since both the Δ and the K^* decay in p waves, their decay distributions in λ must be of the form

$$W(\cos \lambda) \propto 1 + A \cos^2 \lambda. \qquad (9)$$

The values of A for the two resonance are left as free parameters to be varied in the fit.

The choice of a particular production angular momentum barrier is a definite dynamical assumption. One expects rather low partial waves in the final state, especially at our lower momenta, and various assumptions for the final-state orbital angular momentum can be compared with the data. Near threshold the $N\pi$ mass distribution for Δ production is strongly dependent on the angular momentum state in which it is produced. If the final-state $K\Delta$ system is in a relative S wave, the mass spectrum is the product of phase space and the Δ Breit-Wigner function. For nonzero orbital angular momentum in the final state, however, the angular momentum barrier factor will have a dependence on outgoing Δ momentum favoring high momenta, leading to suppression of high $N\pi$ masses. This effect is illustrated in Fig. 6, where the $N\pi$ mass distribution at 864 MeV/c is compared with the predictions for phase space and for Δ production in S, P, and D waves. We have used an angular momentum barrier function of the form

$$f^{\ell}(q) = \left(\frac{q^2}{q^2 + X^2}\right)^{\ell} , \qquad (10)$$

where q is the outgoing kaon momentum in the overall c. m. and where for X we take $X = m_\rho / \sqrt{2} \approx 500$ MeV, as suggested by the ρ-exchange hypothesis for Δ production. Other values of X over 250 MeV give almost indistinguishable results. Of course, as X is decreased to zero, the P- and D-wave curves

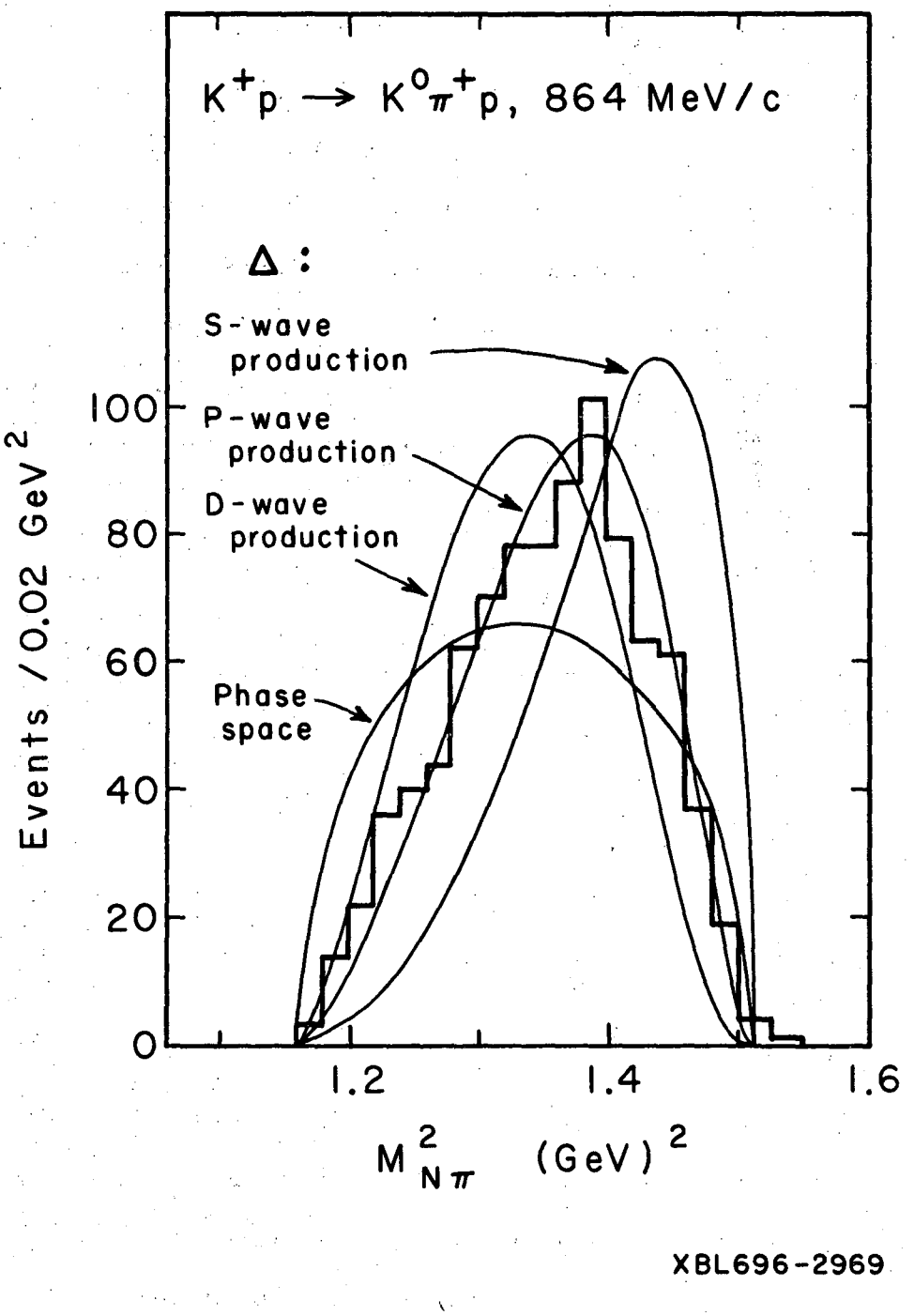

Fig. 6. Experimental $M^2_{N\pi}$ distribution at 864 MeV/c, and the predictions for pure Δ production in S, P, and D waves.

approach the S-wave curve. The data shown in Fig. 6 are inconsistent with any superposition of phase space and S-wave Δ production, and thus require the presence of Δ production in a higher partial wave. On the basis of the excellent agreement of the 864-MeV/c data with the P-wave predictions shown in Fig. 6, we use a P-wave barrier factor for the $K\Delta$ final state[†]. For the K^*N final state we also use a P-wave barrier factor, although with weaker motivation than for the $K\Delta$ final state[††]. For the inverse radius of interaction, we take $X = m_\omega/\sqrt{2}$, because of the evidence of S. Goldhaber et al. favoring ω-exchange in this reaction.[18])

The Dalitz plot density is given under these assumptions by

$$\frac{d^2\sigma}{dM^2_{K\pi}\, dM^2_{N\pi}} = a + b\, I_{K^*} + c\, I_\Delta \ , \qquad (11)$$

[†]We have also shown the production and decay angular distributions to be consistent with production largely through P waves. This is furthermore the prediction of the Stodolsky-Sakurai ρ-exchange model near threshold; see Ref. 9).

[††]We have two reasons for preferring a P-wave K^*N final state: First, the interference models give much better fits with P-wave than with S-wave K^* production. Second, we see strong K^*-Δ interference in the $KN\pi$ Dalitz plots, and such interference can occur only between final states with the same overall spin and parity; hence if the $K\Delta$ final state is dominated by P waves, the K^*N final state is also largely P wave.

where

$$I_{K^*} = BW_{K^*}(1 + A_{K^*} \cos^2 \lambda_{K\pi}) \frac{q_{K^*}^2}{q_{K^*}^2 + m_\omega^2/2} , \quad (12)$$

$$I_\Delta = BW_\Delta (1 + A_\Delta \cos^2 \lambda_{N\pi}) \frac{q_{N\Delta}^2}{q_{N\Delta}^2 + (m_\rho^2/2)} , \quad (13)$$

$$BW = \frac{1}{\sqrt{\pi}} \frac{\Gamma \frac{p_0}{p} m_0}{(m^2 - m_0^2)^2 + (\Gamma m_0)^2} , \quad (14)$$

and $$\Gamma = \Gamma_0 \left(\frac{p^2}{p^2 + m_\pi^2} \Big/ \frac{p_0^2}{p_0^2 + m_\pi^2} \right) \frac{p}{p_0} ; \quad (15)$$

here m_0 and Γ_0 are the nominal resonance mass and width, taken as 1236 MeV and 116 MeV for the Δ, and 891 MeV and 50 MeV for the K^*, m is the appropriate diparticle mass, p_0 and p are the two-body c.m. decay momenta corresponding to m_0 and m, and q_{K^*} and q_Δ are the K^* and Δ momenta in the overall c.m.

b. Empirical interference model

An approximate way to include interference effects in the absence of a detailed calculation is to modify Eq. (12) to

$$\frac{d^2\sigma}{dm_{K\pi}^2 \, dm_{N\pi}^2} = a + b I_{K^*} + c I_\Delta + 2d\left(bc I_{K^*} I_\Delta\right)^{1/2} \cos(\phi_\Delta - \phi_{K^*} + \phi_0). \quad (16)$$

Here I_{K^*} and I_Δ are the same as in Eq. (11), ϕ_{K^*} and ϕ_Δ are the phases of the Δ and K^* amplitudes due to the complex Breit-Wigner amplitude, and ϕ_0 is an additional constant relative phase, to be varied in the fit. The factor d, also varied in the fit, allows for less-than-maximal interference between the K^*N and $K\Delta$ amplitudes. This interference term is a simple, though inexact empirical substitute for a detailed calculation based on a specific choice of amplitudes.

c. P-wave interference model

A constrasting approach which has previously been discussed with a more preliminary version of the data[8]) is to choose definite partial-wave amplitudes for the K^*N and $K\Delta$ final states, and to calculate the resulting Dalitz plot density including the interference†. This is a theoretically more correct procedure, but the choice of partial waves is almost as arbitrary as the assumptions of the empirical interference model. In choosing the Δ amplitude we are guided by the good qualitative agreement between the Δ production and decay angular distributions and the Stodolsky-Sakurai ρ -exchange model. (See Ref. 8.) Since in this model P-wave production of the Δ dominates near threshold, we take for the Δ amplitude the P-wave terms of the ρ -exchange amplitude,

$$a(K\Delta) \approx \vec{q} \times \vec{q}' \cdot (2\vec{p} + i\vec{\sigma} \times \vec{p}) BW_{\Delta} \quad , \qquad (17)$$

where q and q' are the incident and outgoing kaon momenta in the overall c. m., and p is the momentum of the decay pion in the Δ c. m. For K^* production we do not have a clear indication from the data of an appropriate amplitude. We choose a P-wave amplitude analogous to the Δ amplitude,

$$a(K^*N) \sim \vec{q} \times \vec{q}' \cdot \vec{p}\, BW_{K^*} \quad , \qquad (18)$$

where q and q' are the incident K and outgoing K^* momenta in the overall c. m., and p is the decay kaon momentum in the K^* c. m. This predicts for the distribution in the K-K scattering angle α, $W(\cos\alpha) = \sin^2\alpha$, and for the Treiman-Yang angular distribution, $W(\phi) = \sin^2\phi$, in rough agreement with the data. Here too our amplitude corresponds to the P-wave terms of a vector-exchange

†These calculations are described in Ref. 19).

amplitude[†]. The Dalitz plot density is then given by

$$\frac{d^2\sigma}{dm^2_{K\pi}\, dm^2_{N\pi}} \propto \left| a(K^*N) + a(K\Delta)e^{i\phi_0} \right|^2 + \text{phase space} \quad . \tag{19}$$

When this expression is expanded and integrated over the final-state variables other than the Dalitz plot variables, there results

$$\frac{d^2\sigma}{dm^2_{K\pi}\, dm^2_{N\pi}} \propto q^2_{N\pi}\, BW_\Delta \left(1 + \frac{3}{2}\sin^2 \lambda_{N\pi}\right) + q^2_{K\pi}\, BW_{K^*} \sin^2 \lambda_{K\pi}$$
$$+ 2\sqrt{2}\, q_{N\pi} q_{K\pi} \left(BW_{K^*} BW_\Delta\right)^{\frac{1}{2}} \sin \lambda_{N\pi} \sin \lambda_{K\pi} \cos(\phi_\Delta - \phi_{K^*} + \phi_0)$$
$$+ \text{phase space} \quad . \tag{20}$$

The similarity to the empirical interference model should be noted; for $A_\Delta = -0.6$ and $A_{K^*} = -1$, the direct K^*N and $K\Delta$ terms are of identical form, and the interference terms are similar, being (aside from the cos ϕ factor) positive everywhere in the Dalitz plot, and zero at the edges. For other values of A_{K^*} the empirical interference term, although still positive, no longer vanishes at the edges of the Dalitz plot.

B. Results of Fits

In Table 3 we give the results of fitting all our single-pion-production Dalitz plots for fractions of background, Δ production, and, where appropriate, K^* production. In Table 4 we give the corresponding resonance production cross sections, obtained as follows: At 864 and 969 MeV/c and for the $K^+\pi^+n$

[†]Specifically this corresponds to the P-wave part of the vector-exchange amplitude given in Ref. [20]), with the choice of coupling constants $G_V = -G_T$.

Table 3. Fractions of Δ production, K^* production, Δ-K^* interference, and other results of fits to the single-pion-production Dalitz plots. The errors quoted are statistical only, and are modified as described in the text before calculating the cross sections given in Table 4.

Momentum (MeV/c)	Final state	No. of events	Model	χ^2/d.o.f.	d	A_Δ	A_{K^*}	%KΔ	%K^*p	%K^*-Δ int.	% bkgd.	ϕ_0 (deg)
735[a]	$K^0p\pi^+$	108	No-interference	7.0/4	--	--	--	63 ± 36	--	--	37 ± 36	--
785[a]	$K^0p\pi^+$	569	No-interference	23/11	--	--	--	55 ± 9	--	--	45 ± 9	--
864	$K^0p\pi^+$	900	No-interference	9.5/14	--	--	--	75 ± 7	--	--	25 ± 7	--
	$K^+p\pi^0$	301	No-interference	9.6/15	--	--	--	52 ± 15	--	--	48 ± 15	--
	$K^+n\pi^+$	105	No-interference	10.9/6	--	--	--	63 ± 19	--	--	37 ± 19	--
969	$K^0p\pi^+$	1320	No-interference	40.3/20	--	--	--	94 ± 4	--	--	6 ± 4	--
	$K^+p\pi^0$	387	No-interference	18.3/9	--	--	--	54 ± 9	--	--	46 ± 9	--
	$K^+n\pi^+$	155	No-interference	14.5/8	--	--	--	80 ± 14	--	--	20 ± 14	--
1 207	$K^0p\pi^+$	3000	Empir. interf.	47/27	0.53 ± 0.07	-0.50 ± 0.07	0.21 ± 0.18	68 ± 3	21 ± 2	6 ± 2	5 ± 2	38 ± 7
			P-wave interf.	99/30	--	-0.6	-1.	59 ± 2	17 ± 1.5	7 ± 2	18 ± 2	36 ± 5
			No-interference	156/28	--	-0.38 ± 0.07	0.60 ± 0.35	77 ± 2	29 ± 1.7	--	-6 ± 1.4	--
	$K^+p\pi^0$	1131	Empir. interf.	19/22	0.54 ± 0.09	-0.51 ± 0.16	0.40 ± 0.40	45 ± 4	38 ± 3	6 ± 4	11 ± 4	40 ± 10
			P-wave interf.	58/25	--	-0.6	-1.	36 ± 4	34 ± 3	1 ± 4	29 ± 4	48 ± 8
			No-interference	64/23	--	-0.20 ± 0.12	0.90 ± 0.40	56 ± 4	46 ± 3	--	-2 ± 3	--
	$K^+n\pi^+$	359	No-interference	11/14	--	--	--	58 ± 7	--	--	42 ± 7	--
1 367	$K^0p\pi^+$	1521	Empir. interf.	39/22	0.53 ± 0.08	-0.51 ± 0.11	0.70 ± 0.35	57 ± 2.4	32 ± 2	11 ± 2.5	0 ± 2.5	25 ± 7
			P-wave interf.	81/25	--	-0.6	-1.	47 ± 1.6	26 ± 1.9	13 ± 2	14 ± 2	28 ± 6
			No-interference	95/24	--	-0.55 ± 0.10	1.2 ± 0.4	66 ± 2.6	43 ± 2.3	--	-9 ± 1.6	--
1 585	$K^0p\pi^+$	754	Empir. interf.	16/16	0.66 ± 0.13	-0.50 ± 0.20	-0.15 ± 0.30	41 ± 3	43 ± 3	11 ± 3	5 ± 3	29 ± 9
			P-wave interf.	41/19	--	-0.6	-1.	36 ± 2.3	41 ± 2.5	8 ± 3	13 ± 3	43 ± 9
			No-interference	47/17	--	-1.00 ± 0.15	0.00 ± 0.25	52 ± 3	43 ± 3	--	6 ± 3	--

a. Given here are results from a fit to the mass distributions of Fillipas et al., Ref. 22).

Table 4. Summary of cross sections for Δ production, K^* production, and background.

Momentum (MeV/c)	Reaction	σ(KΔ) (mb)	σ(K^*N) (mb)	σ(K^*-Δ int.) (mb)	σ(bkgd) (mb)
735[a]	$K^+p \to K^0\pi^+p$	0.08 ± 0.06	--	--	0.05 ± 0.06
	$\to K\pi N$	0.11 ± 0.08[b]	--	--	--
785[a]	$K^+p \to K^0\pi^+p$	0.19 ± 0.04	--	--	0.15 ± 0.04
	$\to K\pi N$	0.25 ± 0.05[b]	--	--	--
864	$K^+p \to K^0\pi^+p$	0.86 ± 0.12	--	--	0.29 ± 0.12
	$\to K^+\pi^0p$	0.19 ± 0.08	--	--	0.17 ± 0.08
	$\to K^+\pi^+n$	0.08 ± 0.04	--	--	0.05 ± 0.04
	$\to K\pi N$	1.13 ± 0.15	--	--	0.51 ± 0.15
969	$K^+p \to K^0\pi^+p$	2.42 ± 0.19	--	--	0.15 ± 0.15
	$\to K^+\pi^0p$	0.43 ± 0.11	--	--	0.37 ± 0.11
	$\to K^+\pi^+n$	0.24 ± 0.07	--	--	0.06 ± 0.06
	$\to K\pi N$	3.09 ± 0.23	--	--	0.58 ± 0.20
1 207	$K^+p \to K^0\pi^+p$	3.43 ± 0.32	1.06 ± 0.20	0.30 ± 0.30	0.25 ± 0.30
	$\to K^+\pi^0p$	0.81 ± 0.14	0.68 ± 0.11	0.11 ± 0.14	0.20 ± 0.14
	$\to K^+\pi^+n$	0.32 ± 0.06	--	--	0.24 ± 0.06
	$\to K\pi N$	4.56 ± 0.35	1.74 ± 0.23	0.41 ± 0.33	0.69 ± 0.34
1 367	$K^+p \to K^0\pi^+p$	3.05 ± 0.33	1.72 ± 0.24	0.59 ± 0.27	0 ± 0.27
	$\to K\pi N$	4.1 ± 0.4[b]	2.6 ± 0.3[c]	0.8 ± 0.4[d]	--
1 585	$K^+p \to K^0\pi^+p$	2.05 ± 0.34	2.15 ± 0.35	0.55 ± 0.30	0.25 ± 0.30
	$\to K\pi N$	2.7 ± 0.4[b]	3.2 ± 0.4[c]	0.7 ± 0.4[d]	--

a. The numbers given are results of our fit to the data of Filippas et al., Ref. 22.
b. We have used R(all N^* charge states)/R($N^{*++} \to \pi^+p$) = 4/3.
c. We have used R(all K^* charge states)/R($K^{*+} \to K^0\pi^+$) = 3/2.
d. This assumes only isotopic spin conservation, as in b and c above.

final state at 1207 MeV/c we have used the noninterference results, multiplying the errors by $\sqrt{2}$. In the other cases, where the K^* is present, we have used the results of the empirical interference model, doubling the errors. In the following discussion of the results we justify this procedure.

At 864 and 969 MeV/c and for the $K^+n\pi^+$ final state at 1207 MeV/c, the K^* is not present. There we perform a least-χ^2 fit to the $m^2_{N\pi}$ distributions, using an appropriately modified form† of Eq. (11),

$$\frac{d\sigma}{dm^2_{N\pi}} = \left(a + c\ BW(\Delta)\ \frac{q^2_{N\pi}}{q^2_{N\pi} + \frac{m^2_\rho}{2}}\right) \frac{pq_{N\pi}}{m_{N\pi}} \quad , \tag{21}$$

where the symbols have the same meaning as in Eqs. (11) - (15). The errors given in Table 3 are statistical only. To account for possible "theoretical error" in the assumptions of the model, we multiply all errors by $\sqrt{2}$ before computing cross sections. A check on the results can be made by comparing the cross-section ratios for production in reactions (1), (2), and (3) with the 9:2:1 predicted by conservation of isotopic spin. Using the values of Table 4, which include the theoretical error, we find $9:(2.0 \pm 0.8):(0.8 \pm 0.4)$ at 864 MeV/c

†The $KN\pi$ Dalitz plots at 864 and 969 MeV/c show an asymmetry favoring high $K\pi$ mass which cannot be described by Eq. (21). In our partial-wave analysis of the $KN\pi$ final state (R. W. Bland, thesis, University of California, Berkeley, California, to be offered as the next paper of this series) this is attributed to interference between Δ-production and background amplitudes. Filippas et al. (Ref. 22) observed the same effect at 778 MeV/c and arrived at the same explanation. The effect changes sign across the Dalitz plot and so does not affect the $m^2_{N\pi}$ distribution.

and $9:(1.6 \pm 0.4):(0.9 \pm 0.3)$ at 969 MeV/c, in good agreement.

Where the K^* is present the data have been fitted by the least-χ^2 method, dividing the data into rectangular bins in $m^2_{N\pi}$ and $m^2_{K\pi}$. Results for the three different fitting hypotheses are given in Table 3. The noninterference fit is included only to show how strongly the data reject it; this is overwhelming evidence in favor of the presence of K^*-Δ interference. In Fig. 7 we show some results of the noninterference fit, for comparison with the more realistic interference models. We give the $m^2_{K\pi}$ spectra for reaction (1) at 1207 MeV/c, in the bands $1.4 < M^2_{N\pi} < 1.5$ BeV^2 and $1.5 < M^2_{N\pi} < 1.7$ BeV^2. In the first band the interference is maximal at the K^* mass, enhancing the K^* peak. In the second band the interference goes through zero at about the K^* mass, thus shifting the K^* up in mass and suppressing the mass region below the K^*.

The no-interference model clearly does not fit the data in Fig. 7. However, both interference models reproduce the general features of the data. The rather poor χ^2's for the P-wave interference model seen in Table 3 result primarily because the K^* $\cos\lambda_{K\pi}$ distribution predicted by the model, $W(\cos\lambda) \propto \sin^2\lambda$, requires that the K^* production intensity and the interference vanish at the edges of the Dalitz plot, in clear disagreement with the data shown in Fig. 3. The more general empirical interference model gives a better representation of the data, and has by far the lowest χ^2 for all data samples. Even so, the fits to the larger data samples are not very good, probably due to our approximate treatment of the interference.

The empirical interference model results in Table 3 and the cross sections in Table 4 show an encouraging consistency. The Δ-production cross sections in reactions (1), (2), and (3) at 1207 MeV/c are in the ratios $9:(2.1 \pm 0.4):(0.84 \pm 0.15)$, in good agreement with the predicted 9:2:1. For K^*

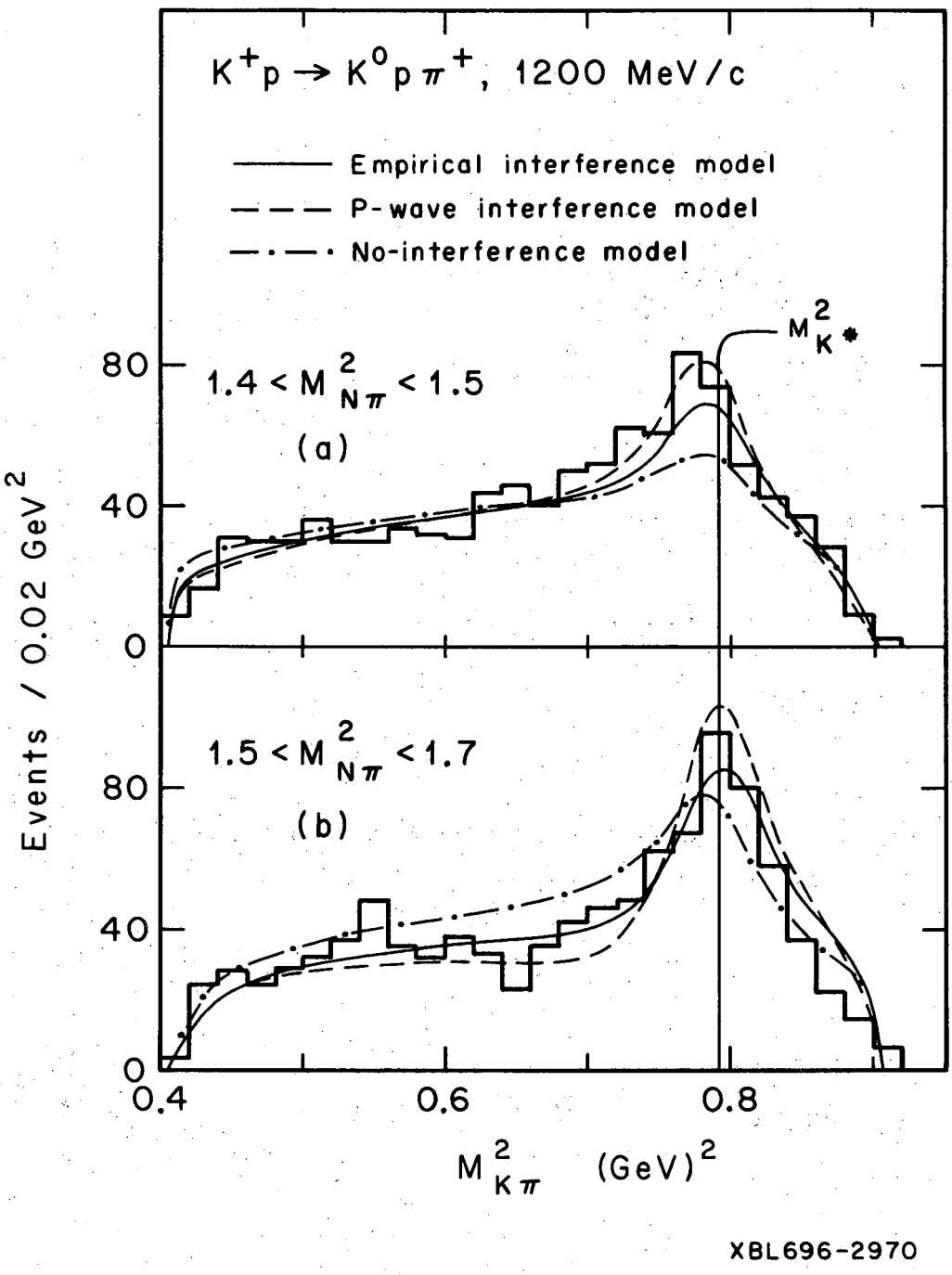

Fig. 7. Experimental $M^2_{K\pi}$ distributions and the predictions of the models discussed in the text.

production the ratio for reactions (1) and (2) is 2:(1.3 ± 0.3), also in good agreement with the predicted 2:1. The parameters d, A_Δ, A_{K^*}, and ϕ_0 should be the same for reactions (1) and (2) at 1207 MeV/c if the model is correct, and the agreement seen in Table 3 is remarkable. In fact, the data from all the fits are consistent with the hypothesis that d, A_Δ, A_{K^*}, and ϕ_0 are constants independent of momentum.

As a further test for the stability of the empirical interference model solutions we have repeated the fit to the 1207-MeV/c $K^0p\pi^+$ data with several modifications of the formalism. The changes and their effects on the χ^2 and parameters are described below; changes in the parameters described as small are less than 1 standard deviation; moderate, 1 to 2 standard deviations; and large, greater than 2 standard deviations.

(a) Replace Δ production barrier factor by 1 (S-wave Δ production)-- χ^2 doubles, moderate change seen in ϕ_0, large changes in other parameters.

(b) Replace K^* production barrier factor by 1 (S-wave K^* production)-- χ^2 doubles, moderate changes seen in parameters. It is interesting to note that, whereas the interference fits are quite sensitive to the production partial waves of the K^*, the noninterference fit is not nearly so sensitive.

(c) Replace Δ barrier factor by $q^2_{N\pi}$ -- χ^2 increases by 6, moderate changes seen in the parameters.

(d) Replace K^* barrier factor by $q^2_{K\pi}$ -- χ^2 unchanged, small changes seen in the parameters.

(e) In the expression for the energy-dependent K^* width (Eq. 15), replace m_π by ∞ -- χ^2 decreases by 1.5, small changes seen in the parameters.

Results a and b above assure us that the P-wave barrier factor is realistic. The less drastic changes c, d, and e are all plausible alternatives to the formalism used, and give us some estimate of the "theoretical uncertainty" in the model. On the basis of these results we double the statistical errors for the empirical interference model fits given in Table 3 when computing cross sections.

From our analysis of the single-pion-production Dalitz plots we draw the following conclusions: (1) strong K^*-Δ interference is required to fit the data, at all momenta; (2) the resonance-decay parameters and the interference parameters, including the relative phase of the K^*N and $K\Delta$ amplitudes, remain constant from the center of the first total-cross-section peak to well above it; (3) the empirical interference model provides a useful parameterization of the single-pion-production Dalitz plots.

B. Double Pion Production

The threshold for reaction (4), $K^+p \rightarrow K^+p\pi^+\pi^-$, occurs at 820 MeV/c beam momentum, but, as is clear from Table 2, the cross section remains very small up to about 1500 MeV/c. There the cross section starts to climb rapidly, with the quasi-two-body final state $K^*(891)\Delta(1236)$ dominating the reaction at higher momenta.[29-32] The effective threshold for double-pion production appears to be the $K^*\Delta$ threshold, occurring at 1750 MeV/c for the central resonance masses, but occurring considerably lower ($\sim$ 1500 MeV/c) for production on the low-mass tails of the resonances. A further indication of $K^*\Delta$ dominance is seen in the relative cross sections for reactions (4) - (6). From conservation of isotopic spin the $K^*\Delta$ final state must divide among

reactions (4) - (8) in the ratios 18:13:2:2:1. Our data at 1367 and 1585 MeV/c are consistent with these ratios.

In Fig. 8 we show a scatter plot of $M_{p\pi^+}$ vs $M_{K^+\pi^-}$ for reaction (4) at 1585 MeV/c, and in Fig. 9 its x and y projections. Double-resonance production is seen on the scatter plot as a clustering of events near the high-mass kinematical limit. The projections show K^* and Δ peaks shifted well below their usual positions, the result of being below the nominal $K^*\Delta$ threshold. To demonstrate that we are indeed seeing double-resonance production below threshold and to determine its cross section we made a fit to the triangle-plot population, assuming an incoherent superposition of four processes: (i) $K^*\Delta$ double-resonance production, (ii) Δ production with a nonresonant $K^+\pi^-$, (iii) K^* production with a nonresonant $p\pi^+$, and (iv) totally nonresonant phase-space background. This gives, for the triangle-plot population,

$$P(M_{K^+\pi^-}, M_{p\pi^+}) = \{\alpha BW(\Delta)BW(K^*) + \beta BW(\Delta) + \gamma BW(K^*) + \delta\} \cdot q_{cm} p_\Delta p_{K^*}, \quad (22)$$

where BW is the p-wave Breit-Wigner function given by Eq. (14), q_{cm} is the Δ or K^* momentum in the overall c.m., and p_Δ and p_{K^*} are the Δ and K^* decay momenta in their respective c.m.'s. The parameters α, β, and γ are varied in the fit, with δ determined by the overall normalization. The triangle plot was divided into 13 rectangular bins, and the best-fit χ^2 was 13.4, for nine degrees of freedom. We also tried several variations on Eq. (22), using different forms for the energy dependence of the resonance widths and multiplying the first term by an angular momentum barrier factor $q_{cm}^2/(q_{cm}^2 + \frac{m_\pi^2}{2})$, corresponding to P-wave $K^*\Delta$ production. These different variations give somewhat different values for α, β, and γ, with comparably good fits. Taking this range of values for the parameters into account in estimating errors, we

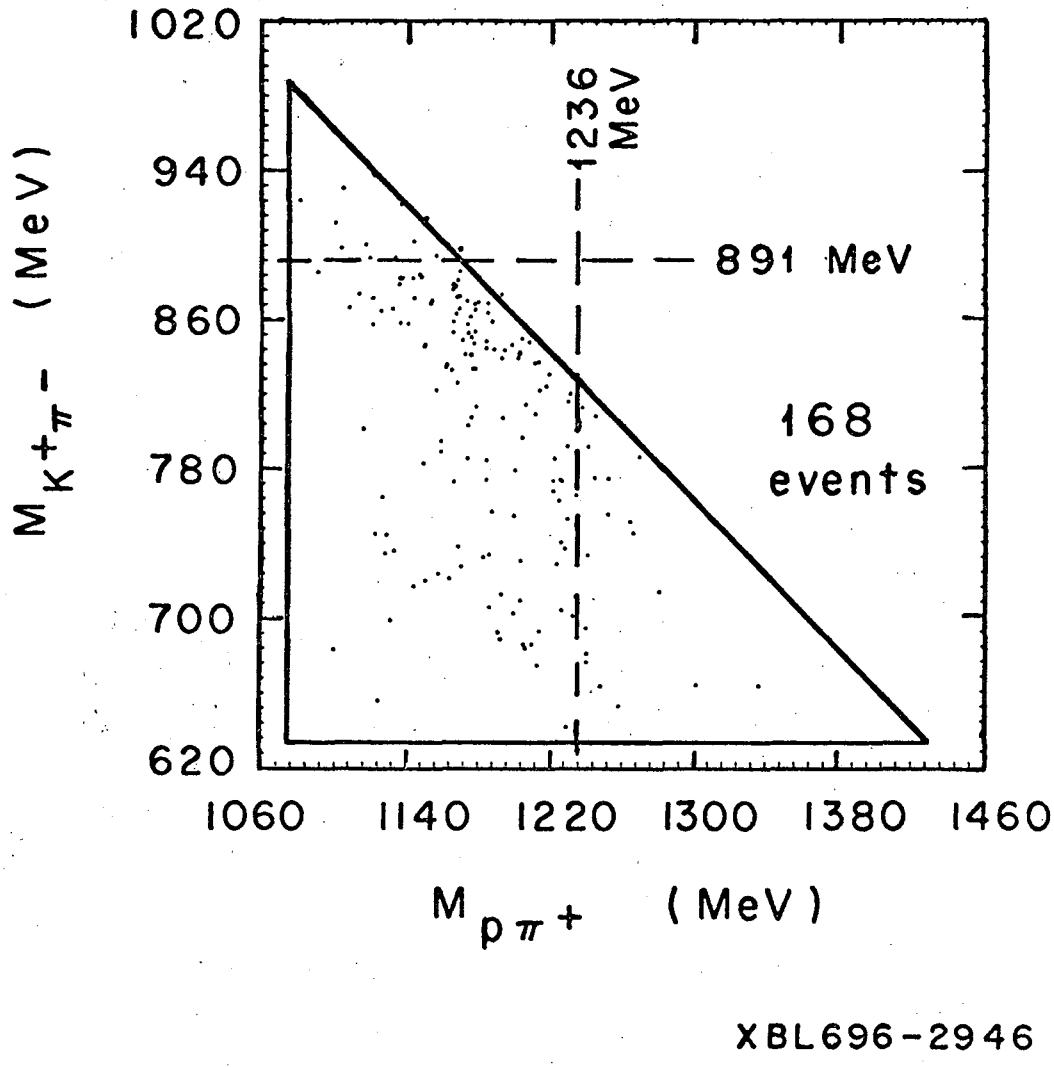

Fig. 8. Triangle plot for the reaction $K^+p \rightarrow K^+p\pi^+\pi^-$ at 1585 MeV/c.

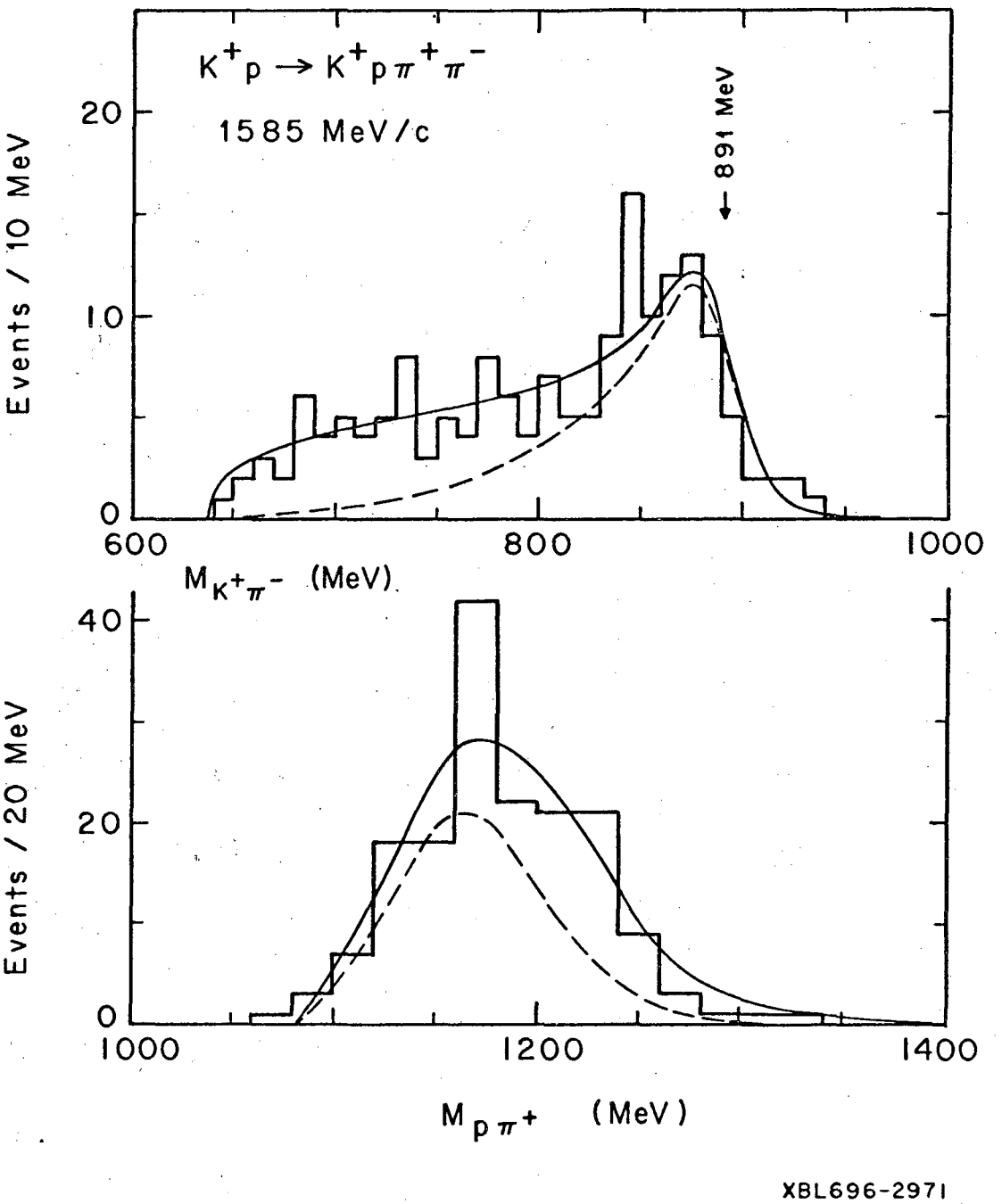

Fig. 9. Mass distributions for the reaction $K^+p \rightarrow K^+p\pi^+\pi^-$ at 1585 MeV/c; the solid curve is the result of the fit described in the text, and the dashed curve is the component attributed to $K^*\Delta$ production alone.

conclude that $K^*\Delta$ production comprises 65 ± 15% of reaction (4), with a cross section of 0.25 ± 0.07 mb. The remainder of the reaction is divided between background and $\Delta K^+\pi^-$, in a ratio not well determined by the fit. The $K^+\pi^-$ and $p\pi^+$ mass spectra corresponding to our fit are drawn on Fig. 9 (solid curves), along with the $K^*\Delta$ component (dashed curves).

In Fig. 10 we give the triangle plot for 57 examples of reaction (4) at 1367 MeV/c. The same fitting procedure at this momentum gave inconclusive results, due to poor statistics and the small span of allowed phase space. However, the cross-section ratios for reactions (4), (5), and (6) suggest that the reaction is still dominated by $K^*\Delta$ production.

5. ENERGY DEPENDENCE OF K^+p CROSS SECTIONS

In Table 5 we give a summary of all available K^+p partial cross sections for final states involving production of up to two pions, from 0.6 to 3.5 BeV/c.[21-33] At those momenta at which only selected final states were measured, the cross sections must be normalized to the number of observed τ decays, and we quote the published cross sections and errors. At momenta at which all final states were measured in the bubble chamber we have renormalized the published data to the counter measurements of the total cross section, according to the following procedure:

A. A counter value for the total cross section is taken from the smooth curve in Fig. 11. The curve is a hand-drawn representation of the counter measurements by Cool et al. and Bugg et al., drawn to join smoothly onto the S-wave effective-range solution of S. Goldhaber et al.[21] below 600 MeV/c. We have ignored the peak-dip structure in the Bugg et al. data near 650 MeV/c.

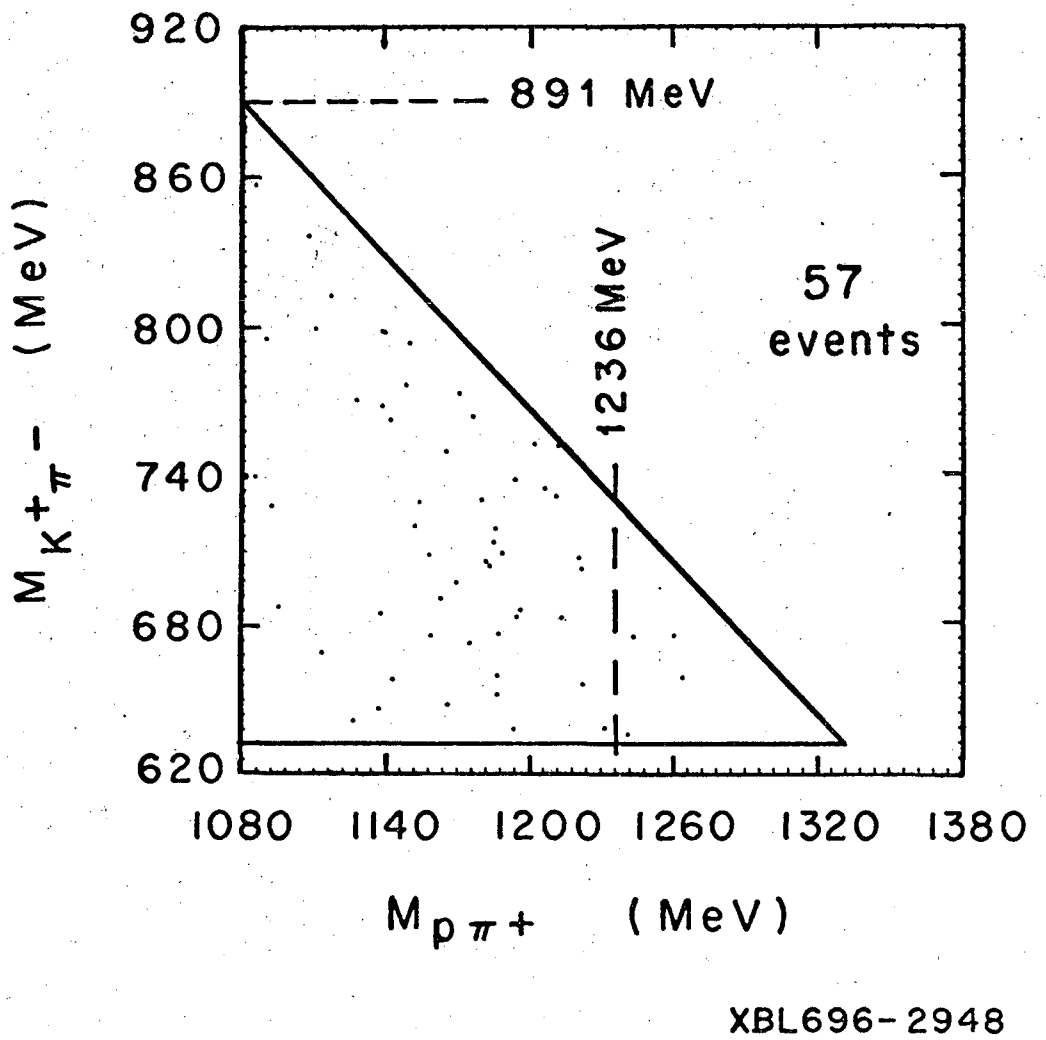

Fig. 10. Triangle plot for the reaction $K^+p \rightarrow K^+p\pi^+\pi^-$ at 1367 MeV/c.

Table 5. K^+p cross sections from 0.6 to 3.5 BeV/c.

Beam Momentum (BeV/c)	K^+p (nuclear)	$K^0p\pi^+$	$K^+p\pi^0$	$K^+n\pi^+$	$KN\pi$	$K^+p\pi^+\pi^-$	$K^0p\pi^+\pi^0$	$K^0n\pi^+\pi^+$	$KN\pi\pi$[a]	Total	References
0.642	12.2 ± 0.7				0.06 ± 0.03					12.3 ± 0.7	21
0.735		0.13 ± 0.01	0.03 ± 0.01	0.02 ± 0.01	0.18 ± 0.01						22
0.785	12.1 ± 0.3	0.34 ± 0.03	0.11 ± 0.01	0.07 ± 0.01	0.52 ± 0.03					12.6 ± 0.3	22, 23
0.810	12.1 ± 0.4	0.63 ± 0.08	0.22 ± 0.05	0.11 ± 0.04	0.96 ± 0.10					13.1 ± 0.4	24, 25
0.864	12.0 ± 0.3	1.15 ± 0.06	0.36 ± 0.03	0.13 ± 0.02	1.64 ± 0.07					13.6 ± 0.3	
0.910		2.1 ± 0.2									26
0.969	11.7 ± 0.2	2.57 ± 0.12	0.80 ± 0.07	0.30 ± 0.04	3.67 ± 0.14					15.35 ± 0.22	
1.14		4.6 ± 0.3									27
1.207	10.9 ± 0.2	5.04 ± 0.15	1.80 ± 0.10	0.56 ± 0.06	7.40 ± 0.17	0.026 ± 0.010			0.029 ± 0.011	18.32 ± 0.12	
1.367		5.4 ± 0.3				0.065 ± 0.012	0.060 ± 0.018	0.009 ± 0.009	0.147 ± 0.025		
1.455	9.5 ± 0.3	4.9 ± 0.3	1.9 ± 0.2	1.34 ± 0.10	8.16 ± 0.30	0.15 ± 0.04	0.08 ± 0.05	0.02 ± 0.02	0.28 ± 0.07	17.94 ± 0.10	28
1.585		5.0 ± 0.4				0.38 ± 0.05	0.32 ± 0.07	0.08 ± 0.03	0.86 ± 0.10		
1.96	6.8 ± 0.5	4.2 ± 0.5	1.9 ± 0.3	1.5 ± 0.3	7.4 ± 0.5	1.64 ± 0.20	1.24 ± 0.20	0.32 ± 0.10	3.5 ± 0.3	17.61 ± 0.07	29
2.26		2.6 ± 0.3				1.7 ± 0.2					30
2.65		2.7 ± 0.3				2.5 ± 0.2	1.9 ± 0.2	0.64 ± 0.12	5.5 ± 0.4		31
2.97	4.8 ± 0.4	2.1 ± 0.3				2.3 ± 0.3	2.1 ± 0.3	0.6 ± 0.2	5.5 ± 0.7		32
2.97		2.3 ± 0.3	1.1 ± 0.2	1.0 ± 0.2	4.4 ± 0.4						32
3.46	4.4 ± 0.4	1.87 ± 0.09	1.32 ± 0.07	0.8 ± 0.4	4.0 ± 0.4	2.1 ± 0.2	2.2 ± 0.2	0.5 ± 0.1	5.3 ± 0.5		33

a. The $KN\pi\pi$ cross section is calculated with K^*-Δ dominance assumed -- see text.

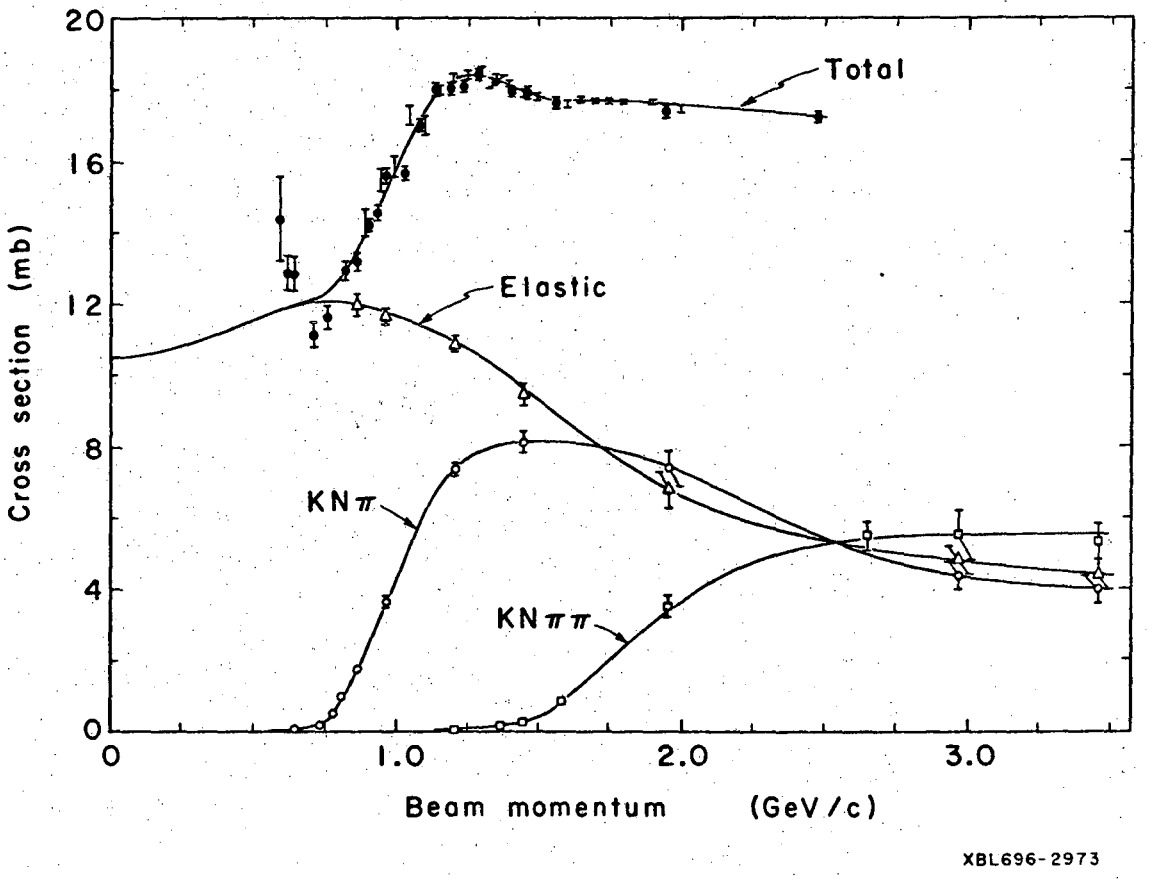

Fig. 11. K^+p total, elastic, single-pion-production, and double-pion-production cross sections as functions of beam momentum.

For the error on the counter total cross section we take the smaller of the errors from the two experiments. Below 900 MeV/c, where our smoothed total cross section curve begins to differ from the Bugg et al. measurements, we increase the errors on the counter measurements appropriately.

B. The counter and bubble chamber cross sections are then averaged statistically, assuming the bubble chamber partial cross sections to be statistically independent. Specifically, if there are N partial cross sections measured by the bubble chamber experiment, we perform a one-constraint N-parameter least-squares fit to the N + 1 data values. Two further remarks on the compilation of the data should be made:

(a) At momenta up to 1.0 GeV/c we quote nuclear cross sections, excluding Coulomb effects in elastic scattering; the correction is obtained from published partial wave solutions.[21, 24] Above 1.0 GeV/c the correction is assumed to be negligible.

(b) Since only three of the five $KN\pi\pi$ final states are accessible to kinematic fitting, we have obtained a total $KN\pi\pi$ cross section by assuming that the $KN\pi\pi$ final states are dominated by $K^*\Delta$ production, a supposition which has good experimental support even down to 1.58 GeV/c, near threshold for $K^*\Delta$. On this assumption the unseen final states represent 8% of the total $KN\pi\pi$ production and the correction is small.

In Fig. 11 we show the cross sections for the processes

$$K^+p \to K^+p \ ,$$

$$K^+p \to KN\pi \ ,$$

and

$$K^+p \to KN\pi\pi$$

from 640 MeV/c to 3.5 GeV/c, and in Fig. 12 the resonance production cross sections,

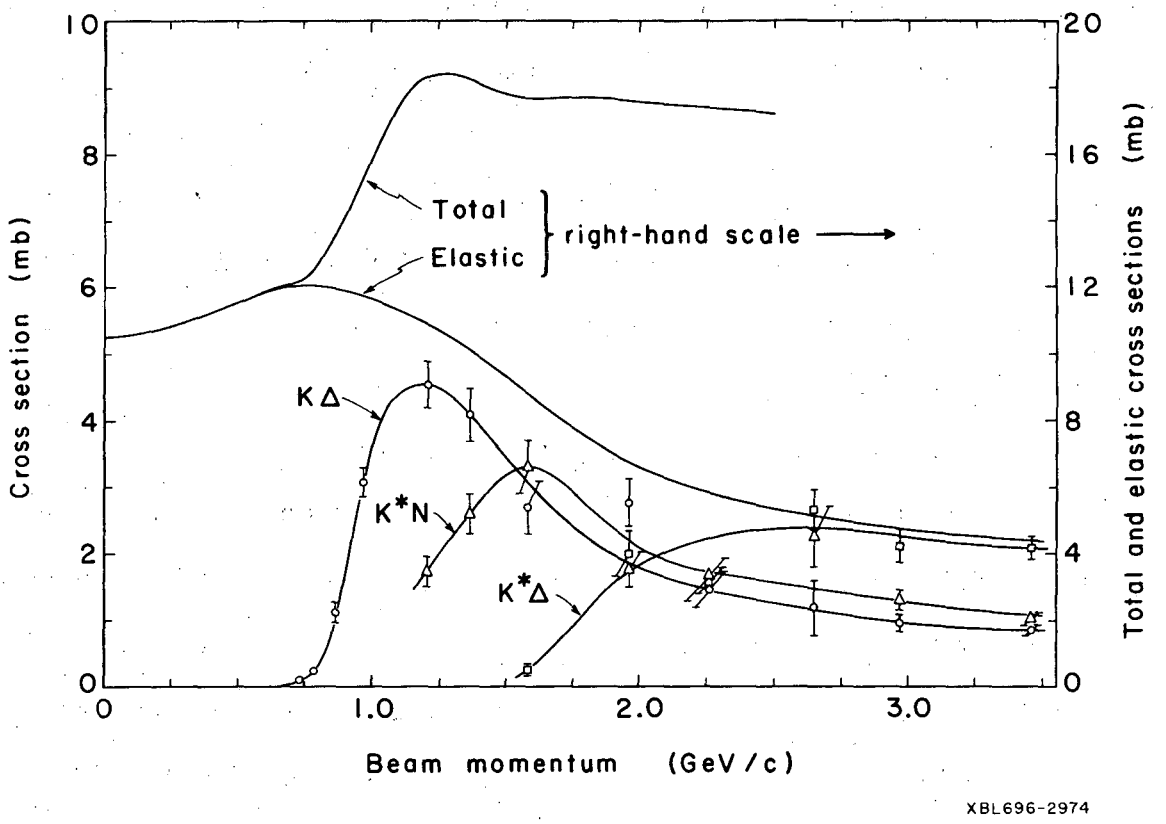

Fig. 12. Cross sections for $K\Delta$, K^*N, and $K^*\Delta$ production in the K^+p channel, as functions of beam momentum.

$$K^+p \rightarrow K\Delta(1236) \quad ,$$
$$K^+p \rightarrow K^*(891)p \quad ,$$
$$K^+p \rightarrow K^*(891)\Delta(1236) \quad .$$

These data can be summarized as follows:

(a) The elastic scattering cross section drops steadily from about 12 mb at 800 MeV/c to 4.4 mb at 3.5 GeV/c.

(b) The single-pion-production channels dominate the inelastic processes up to 1.5 GeV/c. They rise rapidly as the K^+ momentum increases above 0.8 GeV/c, reach a broad maximum of about 8 mb near 1.45 GeV/c, and then slowly and smoothly drop off.

(c) The two-pion production remains very small from threshold (0.82 GeV/c) to about 1.5 GeV/c, and then rises abruptly. Presumably the explanation of this behavior lies in the dominance of $K^*\Delta$ production, whose effective threshold lies near 1.6 GeV/c.

(d) Three-pion production (not shown in Fig. 11) is negligible up to 2 GeV/c.

(e) Δ and K^* production rise rapidly from their thresholds, then fall off somewhat more slowly.

(f) Δ-K^* double-resonance production rises slowly from its threshold to a broad maximum above 2.5 GeV/c.

The curves in Fig. 11 are smooth hand-drawn representations of the data. Below 2 GeV/c they are constrained so that the sum of K^+p, $KN\pi$, and $KN\pi\pi$ cross sections equals the total cross sections. The remarkable feature is that the structure at 1.25 GeV/c is very well reconstructed by the sum of three structureless channel cross sections. The interpretation of that structure in terms of contributions from the various channels can then be expressed in the following terms: The rise above 0.8 GeV/c is associated with the rapidly

rising single-pion cross section, the maximum being reached when this rate of rise is just balanced by the rate of drop of the elastic cross section. This maximum is followed by a drop as the single-pion cross section levels off and the elastic cross section continues to decrease. Finally, this drop is arrested when the two-pion cross section begins to rise at about 1.5 GeV/c. Thus the structure in the total cross section at 1.25 GeV/c does not arise from structure in any single partial cross section. Rather it is a consequence of the sharp rises of the single- and double-pion-production channels at widely separated thresholds. Although the available data are not sufficient to prove it, it is quite reasonable to suppose that the additional small structure observed by Cool et al. may be a consequence of the fact that the 3π cross section becomes significant only at K momenta substantially above 2 GeV/c, at which point the 2π channel has ceased rising and the combined KN, $KN\pi$, and $KN\pi\pi$ cross sections are rapidly dropping.

It should be emphasized that this interpretation of the structure in the total cross section is at variance with the conventional resonance interpretation but completely in accordance with the fact that the detailed behavior of angular distributions and polarizations in the inelastic channels varies slowly and smoothly even through the momentum region in which the structure in the total cross section occurs.[9]

6. ACKNOWLEDGMENTS

We thank the 25-inch bubble chamber crews and the Bevatron staff for their help during the experimental run at the Bevatron, and Howard White, Jr. and the Data Handling Group for their aid in analyzing the events. We also

gratefully acknowledge the efforts of our scanning, measuring, and programming staff.

REFERENCES

1) V. Cook, D. Keefe, L. T. Kerth, P. G. Murphy, W. A. Wenzel, and T. F. Zipf, Phys. Rev. Letters 7, 182 (1961).

2) R. L. Cool, G. Giacomelli, T. F. Kycia, B. A. Leontić, K. K. Li, A. Lundby, and J. Teiger, Phys. Rev. Letters 17, 102 (1966).

3) R. J. Abrams, R. L. Cool, G. Giacomelli, T. F. Kycia, B. A. Leontić, K. K. Li, and D. N. Michael, Phys. Rev. Letters 19, 259 (1967).

4) D. V. Bugg, R. S. Gilmore, K. M. Knight, D. C. Salter, G. H. Stafford, E. J. N. Wilson, J. D. Davies, J. D. Dowell, P. M. Hattersley, R. J. Homer, A. W. O'Dell, A. A. Carter, R. J. Tapper, and K. F. Riley, Phys. Rev. 168, 1466 (1968).

5) R. W. Bland, G. Goldhaber, and G. H. Trilling, K^+p Elastic Scattering at 864, 969, and 1207 MeV/c, submitted to Physics Letters

6) J. Brown, R. Bland, M. Bowler, G. Goldhaber, S. Goldhaber, A. Hirata, J. Kadyk, V. Seeger, and G. Trilling, in Proceedings of the XII International Conference on High Energy Physics, Dubna (Atomizdat, Moscow, 1966), p. 715.

7) M. Bowler, R. Bland, J. Brown, G. Goldhaber, J. Kadyk, V. Seeger, and G. Trilling, Lecture presented at the Oxford International Conference on Elementary Particles, Oxford, England, September 19-25, 1965 (UCRL-16370, Dec. 1965, unpublished).

8) R. Bland, M. Bowler, J. Brown, G. Goldhaber, S. Goldhaber, J. Kadyk, and G. Trilling, Phys. Rev. Letters 17, 939 (1966).

9) R. Bland, M. Bowler, J. Brown, G. Goldhaber, S. Goldhaber, V. Seeger, and G. H. Trilling, Phys. Rev. Letters 18, 1077 (1967).

10) R. B. Bell, R. W. Bland, M. G. Bowler, J. L. Brown, R. P. Ely, S. Y. Fung, G. Goldhaber, A. A. Hirata, J. A. Kadyk, J. Louie, C. T. Murphy, J. S. Sahouria, V. H. Seeger, W. M. Smart, and G. H. Trilling, Lawrence Radiation Laboratory Report UCRL-11527 (1964).

11) H. S. White, T. Aronstein, C. Osborne, N. Webre, and W. G. Moorhead, Nuclear Instr. Methods 20, 393 (1963).

12) R. W. Bland (thesis), Lawrence Radiation Laboratory Report UCRL-18131, March 1968.

13) V. H. Seeger (thesis), Lawrence Radiation Laboratory, (in preparation).

14) B. H. Hall, R. W. Bland, G. Goldhaber, and G. H. Trilling, (Lawrence Radiation Laboratory), private communication, 1969.

15) J. L. Brown, Trilling-Goldhaber Internal Report TN-29, 1964, Lawrence Radiation Laboratory, Berkeley, California (unpublished).

16) A. Rosenfeld, N. Barash-Schmidt, A. Barbaro-Galtieri, L. Price, P. Söding, C. Wohl, M. Roos, and W. Willis, Data On Particles and Resonant States, Lawrence Radiation Laboratory Report UCRL-8030, Part I, Jan. 1968.

17) Trilling-Goldhaber Group Memo TG-170, Lawrence Radiation Laboratory, Berkeley, California (unpublished).

18) S. Goldhaber, J. L. Brown, I. Butterworth, G. Goldhaber, A. A. Hirata, J. A. Kadyk, and G. H. Trilling, Phys. Rev. Letters 15, 737 (1965).

19) George Trilling, Lawrence Radiation Laboratory Trilling-Goldhaber Group Memo TG-149 (unpublished).

20) J. D. Jackson and H. L. Pilkuhn, Nuovo Cimento 33, 906 (1964).

21) 642 MeV/c--S. Goldhaber, W. Chinowsky, G. Goldhaber, W. Lee, T. O'Halloran, T. F. Stubbs, G. M. Pjerrou, D. H. Stork, and H. K. Ticho, Phys. Rev. Letters 9, 135 (1962).

22) 735- and 785-MeV/c $K^+p \rightarrow K\pi N$--T. A. Filippas, V. P. Henri, B. Jongejans, F. Krammer, J. M. Perreau, S. Focardi, A. Minguzzi-Ranzi, L. Monari, G. Saltini, P. Serra, E. Barrelet, E. Huffer, and F. Muller, Nuovo Cimento 51A, 1053 (1967).

23) 785-MeV/c K^+p elastic scattering--S. Focardi, A. Minguzzi-Ranzi, L. Monari, G. Saltini, P. Serra, T. A. Filippas, and V. P. Henri, Physics Letters 24B, 314 (1967).

24) 810-MeV/c K^+p elastic scattering--T. F. Stubbs, H. Bradner, W. Chinowsky, G. Goldhaber, S. Goldhaber, W. Slater, D. M. Stork, and H. K. Ticho, Phys. Rev. Letters 7, 188 (1961).

25) 810-MeV/c $K^+p \rightarrow K\pi N$--J. Fisk, H. K. Ticho, D. H. Stork, W. Chinowsky, G. Goldhaber, S. Goldhaber, and T. F. Stubbs, Proceedings of the 1962 International Conference on High-Energy Physics at CERN, J. Prentki, editor (CERN, Geneva 23, Switzerland).

26) 910 MeV/c--B. Kehoe, Phys. Rev. Letters 11, 93 (1963).

27) 1140 MeV/c--E. Boldt, J. Duboc, N. H. Duong, P. Eberhard, R. George, V. P. Henri, F. Levy, J. Poyen, M. Pripstein, J. Crussard, and A. Tran, Phys. Rev. 133, B220 (1964).

28) 1450 MeV/c--A. Bettini, M. Cresti, S. Limentani, L. Perruzzo, R. Santangelo, D. Locke, D. J. Crennell, W. T. Davies, and P. B. Jones, Physics Letters 16, 83 (1965); G. B. Chadwick, D. J. Crennell, W. T. Davies, M. Derrick, J. H. Mulvey, P. B. Jones, D. Radojicic,

C. A. Wilkinson, A. Bettini, M. Cresti, S. Limentani, L. Perruzzo, and R. Santangelo, Physics Letters 6, 309 (1963).

29) 1.96 GeV/c: cross sections and elastic scattering--W. Chinowsky, G. Goldhaber, S. Goldhaber, T. O'Halloran, and B. Schwarzschild, Phys. Rev. 139B, 1411 (1965); $K^+p \rightarrow KN\pi$--S. Goldhaber, W. Chinowsky, G. Goldhaber, and T. O'Halloran, Phys. Rev. 142, 913 (1966); $K^+p \rightarrow KN\pi\pi$--G. Goldhaber, W. Chinowsky, S. Goldhaber, W. Lee, and T. O'Halloran, Phys. Letters 6, 62 (1963).

30) 2.26 GeV/c--F. Bomse, S. Borenstein, J. Cole, D. Gillespie, R. Kraemer, G. Luste, I. Miller, E. Moses, A. Pevsner, R. Singh, and R. Zdanis, Phys. Rev. 158, 1281, 1298 (1967).

31) 2.65 GeV/c--R. Newman, W. Chinowsky, J. Schultz, W. B. Johnson, and R. R. Larsen, Phys. Rev. 158, 1310 (1967).

32) 2.97 GeV/c: $K^+p \rightarrow K^0p\pi^+$--M. Ferro-Luzzi, R. George, Y. Goldschmidt-Clermont, V. P. Henri, B. Jongejans, D. W. G. Leith, G. R. Lynch, F. Muller, and J.-M. Perreau, Nuovo Cimento 36, 1101 (1965); $K^+p \rightarrow KN\pi$--P. Sällström, G. Otter, and G. Ekspong, Nuovo Cimento 49, 348 (1967), P. Sällström and G. Blomqvist, Arkiv für Fysik 37, 463 (1968); $K^+p \rightarrow KN\pi\pi$--M. Ferro-Luzzi, R. George, Y. Goldschmidt-Clermont, V. P. Henri, B. Jongejans, D. W. G. Leith, G. R. Lynch, F. Muller, and J.-M. Perreau, Nuovo Cimento 39, 417 (1965); $K^+p \rightarrow K^+p$--J. Debaisieux, F. Grard, J. Heughebaert, L. Pape, R. Windmolders, R. George, Y. Goldschmidt-Clermont, V. P. Henri, D. W. G. Leith, G. R. Lynch, F. Muller, J.-M. Perreau, G. Otter, and P. Sällström, Nuovo Cimento 43A, 142 (1966).

33) 3.46 GeV/c: $K^+p \rightarrow KN\pi$--W. de Baere, J. Debaisieux, P. Dufour, F. Grard, J. Heughebaert, L. Pape, P. Peeters, F. Verbeure, R. Windmolders, Y. Goldschmidt-Clermont, V. P. Henri, B. Jongejans, A. Moisseev, F. Muller, J.-M. Perreau, A. Prokeš, and V. Yarba, Nuovo Cimento 51A, 401 (1967); $K^+p \rightarrow KN\pi\pi$--R. George, Y. Goldschmidt-Clermont, V. P. Henri, B. Jongejans, M. Krammer, F. Muller, J.-M. Perreau, W. de Baere, J. Debaisieux, P. Dufour, F. Grard, J. Heughebaert, L. Pape, P. Peeters, F. Verbeure, and R. Windmolders, Nuovo Cimento 49A, 9 (1967); $K^+p \rightarrow K^+p$--W. de Baere, J. Debaisieux, P. Dufour, F. Grard, J. Heughebaert, L. Pape, P. Peeters, F. Verbeure, R. Windmolders, R. George, Y. Goldschmidt-Clermont, V. P. Henri, B. Jongejans, D. W. G. Leith, A. Moisseev, F. Muller, J.-M. Perreau, and V. Yarba, Nuovo Cimento 45A, 885 (1966).

TECHNICAL INFORMATION DIVISION
LAWRENCE RADIATION LABORATORY
UNIVERSITY OF CALIFORNIA
BERKELEY, CALIFORNIA 94720